ChemComm

COMMUNICATION

View Article Online
View Journal | View Issue

Cite this: *Chem. Commun.*, 2018, **54**, 6895

Received 27th March 2018,
Accepted 30th April 2018

DOI: 10.1039/c8cc02436g

rsc.li/chemcomm

Proton and ammonia intercalation into layered iron chalcogenides†

Xiuquan Zhou,[ab] Brandon Wilfong,[ab] Sz-Chian Liou,[c] Halyna Hodovanets,[b] Craig M. Brown[d] and Efrain E. Rodriguez*[ab]

Structurally related to the iron-based superconductors, two new intercalated iron chalcogenides $(H_{0.5}NH_3)Fe_2Ch_2$ where Ch = S, Se have been prepared. By topochemical conversion, the protons were exchanged by lithium to form $(Li_{0.5}NH_3)Fe_2Ch_2$. Hydrogen bonding plays a significant role in the guest–host interactions of these intercalated phases.

Superconducting FeSe has rich intercalation chemistry owing to weak van der Waals interactions between the sheets of edge-sharing $FeSe_4$ tetrahedra. Upon intercalation, its superconducting critical temperature (T_c) can be increased from 8.5 K to (42–44) K.[1–5] The species that readily intercalate into the FeSe sheets can be classified into two categories: (I) simple cations such as K^+ and Rb^+ and (II) partially charged Lewis acid–base adducts such as metal cations coordinated to amine or hydroxo groups.[6,7] In the former case, ionic interactions predominate, whereas in the latter, the reduced charge of the adducts causes additional interactions between the FeSe host and its guest adduct. We demonstrate here that hydrogen bonding is a relevant guest–host interaction in iron chalcogenides and that intercalated phases can be prepared without the need for metal cations as Lewis acids.

Previous work has shown that FeSe intercalates adducts including Li^+ with bases such as OH^-,[4] ammonia,[3] diamines $H_2N(CH_2)_nNH_2$ (n = 2, 3, 6),[8–10] and pyridine.[11] A common denominator shared by these adducts is a strong hydrogen donating group such as –OH or $–NH_2$. Neutron diffraction studies (including on deuterium substituted specimens) have revealed that the –OH and $–NH_2$ groups are directed towards the FeSe layers. These structural studies have reported H(D)···Se distances of 2.75 Å,[3,12] 2.60 Å[10] and 3.05–3.10 Å[13,14,15] for Li·ammonia, Na·ethylenediamine (EDA), and Li·OH adducts, respectively, and (2.62–3.00) Å[16] for EDA coordinated $FeSe_2$ chains. The effect of hydrogen bonding becomes more evident when looking beyond FeSe. Its structural analogues, such as FeS, CoSe and $FeTe_{0.6}Se_{0.4}$, can all be similarly intercalated by adducts with strong hydrogen donating groups.[17–21]

If hydrogen bonding is indeed a major driving force for intercalation, then intercalated FeCh free of alkali metals should be possible. To date, most adducts have been intercalated under highly reducing conditions such as alkali or alkali earth metals dissolved in liquid ammonia (*i.e.* the Birch reduction), or mild hydrothermal conditions with concentrated alkali metal hydroxides.[7] Therefore, finding an alkali-metal-free route would prove that new and metastable phases of layered chalcogenides can be obtained without the need for alkali metal co-intercalation.

First, we targeted ammonia-intercalated FeCh (**1** in Fig. 1) without any alkali metals. Ammonia is small, polar, and capable of forming

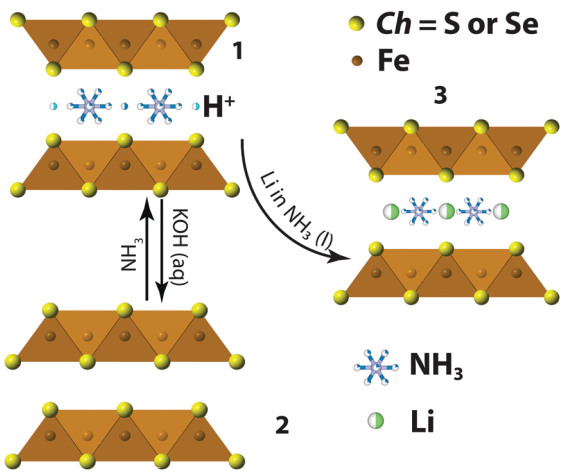

Fig. 1 Crystal structure of $(H_{0.5}NH_3)Fe_2Ch_2$ (**1**) and its topochemical conversion to related phases FeCh (**2**) and $(Li_{0.5}NH_3)Fe_2Ch_2$ (**3**).

[a] *Department of Chemistry and Biochemistry, University of Maryland, College Park, MD 20742, USA. E-mail: efrain@umd.edu*
[b] *Center for Nanophysics and Advanced Materials, Department of Physics, University of Maryland, College Park, MD 20742, USA*
[c] *AIM Lab, Maryland NanoCenter, University of Maryland, College Park, MD 20742, USA*
[d] *NIST Center for Neutron Research, National Institute of Standards and Technology, Gaithersburg, MD 20899, USA*

† Electronic supplementary information (ESI) available. See DOI: 10.1039/c8cc02436g

strong hydrogen bonds. Our previous hydrothermal synthesis included Fe metal powder with a sulfur source under strong basic conditions as an effective and versatile means to intercalate different alkali bases into FeS.[17] To prepare our title compounds, we first utilized under hydrothermal conditions an organic metal-free base – guanidine, $(NH_2)_2C{=}NH$,[22] to afford strong basic conditions. Guanidine, analogous to urea, exhibits a basicity (pK_a = 13.6) comparable to KOH in aqueous solution.[23] Therefore, it can effectively digest the Fe metal powder under hydrothermal conditions. Furthermore, it rapidly decomposes to NH_3 and CH_4 above 150 °C.[24] By keeping the hydrothermal conditions mild (T < 150 °C), ammonia can be slowly released as FeS sheets crystallize *in situ*.

Our targeted synthesis afforded two new intercalated phases using either large amounts of excess guanidine or saturated ammonia water at 125 °C for 3–5 days. Both their powder X-ray diffraction (PXRD) patterns can be indexed to the same body-centered tetragonal space group (*I*4/*mmm*). The unit cell resembles that of the $ThCr_2Si_2$-type (or 122-type) structure seen for $K_xFe_2Ch_2$. Using the 122-type structural model, we successfully fitted both PXRD patterns with a phase of composition NFe_2Ch_2 as shown in Fig. S1 (ESI†). Rietveld refinement led to occupancies near unity for the N, Fe and Ch sites. We could not resolve the positions of hydrogen atoms with PXRD, but it is obvious that hydrogens must be added to the formula NFe_2Ch_2 since this compound does not contain free nitrogen nor N^{3-} species. Thus, the real formula is likely to be $NH_xFe_2Ch_2$ for $3 < x < 4$.

To definitively determine the crystal structure and composition of $NH_nFe_2Ch_2$, a partially deuterated sulfide sample was prepared using a 2 : 1 ratio of D_2O to 25% $(NH_4)_2S$(aq) and studied by neutron powder diffraction (NPD). The deuteration helped reduce the incoherent scattering from hydrogen so that minor reflections would not be overwhelmed by background. Although all reflections of the NPD data were accounted for by the NFe_2Ch_2 structural model from PXRD, we still observed a large discrepancy between the observed and calculated intensities (Fig. 2, top panel). Obviously, ammonia molecules rather than free nitrogen located at the cell corners or the 2*a* site (0, 0, 0) were necessary to better model the neutron data.

Our first model for locating the hydrogen was to place H/D atoms within a 1 Å radius of the N atom, which would place them in both the 8*i* (x, 0, 0) and 16*m* (x, x, z) sites. We also assumed that the H and D atoms were disordered on these two sites. Notwithstanding a noticeable improvement in the structural refinement, this new addition to the crystallographic model was not adequate. Fourier difference maps revealed significant discrepancies in the nuclear densities located at the edge-center of the unit cell, which would correspond to the 2*b* site (0, 0, 1/2).

Our second model placed H/D atoms on the 2*b* site and allowed the respective occupancies to vary independently. Interestingly, addition of D at the 2*b* site improved the statistics significantly, while addition of any H at this site worsened the fit, particularly for the (002) reflection. It is important to recall that H has a coherent neutron scattering length of −3.7423(12) fm, while D has a scattering length of 6.674(6) fm. Thus, a high contrast exists between the two isotopes for their contribution to the structure factors. Unlike the 8*i* and 16*m* sites where both H and D atoms coexist, the 2*b* site is exclusively populated by D. Our final model therefore has D exclusively at the 2*b* site, and a H/D mixture on the 8*i* and 16*m* sites.

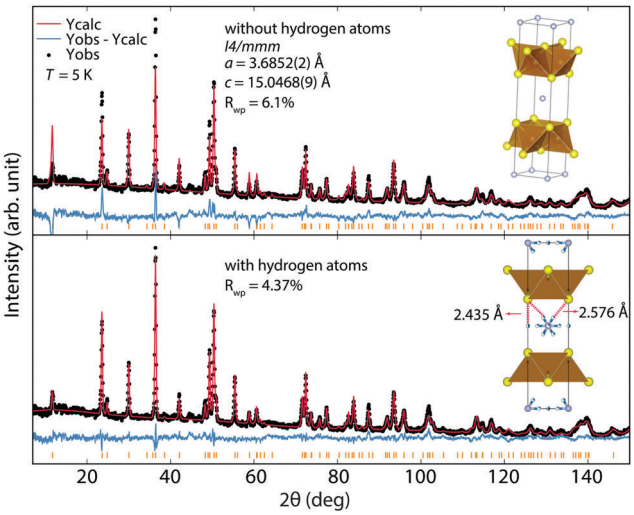

Fig. 2 Neutron powder diffraction (NPD) pattern of ammonia-intercalated FeS collected at 5 K showing Rietveld refinement without (top) and with (bottom) considering the hydrogen or deuterium positions.

The final Rietveld refinement to the overall NPD pattern is shown in Fig. 2 (bottom panel). The proposed chemical formula is $(D_{0.48(2)}NH_{1.59(7)}D_{1.45(4)})Fe_{1.94(2)}S_2$. All the structural parameters are gathered in Table S1 (ESI†). Although we did not carry out NPD studies of the selenide analogue, it is likely that both chalcogenides share a similar structure and composition. Hence, the ammonia-intercalated FeCh can be described using a generic formula of $(H_{0.5}NH_3)Fe_2Ch_2$, where the proton is explicitly written to distinguish it from the amine hydrogen.

The structural solution for $(H_{0.5}NH_3)Fe_2Ch_2$ shares several similarities with the structure of the Li·amine adduct intercalated into FeSe by Clarke and co-workers.[3] In both compounds the cations are found at the cell edges between the Se^{2-} anions of the FeSe sheets. There are some interesting differences, however. In our compound, the 2*b* site is now populated by a proton instead of Li^+ and the 4*c* site (1/2, 0, 0) is now empty rather than being occupied by Li^+. This suggests that even without alkali metals, ammonia and excess protons alone provide a sufficient driving force for intercalation through hydrogen bonding and some Coulombic attraction between the H^+ and $(FeCh)^{0.25-}$ layers.

Besides the location of the cations, the nature of the intercalated amine groups is different between our title compounds and the superconductor prepared by Burrard-Lucas *et al.*[3] The formula of their phase is $Li_{0.6}(ND_2)_{0.2}(ND_3)_{0.8}Fe_2Se_2$, which suggests that approximately 20% of the amine group is actually an amide. The extra Li^+ is therefore charge compensated by anionic $(ND_2)^-$ groups for a total charge transfer of $0.2e^-$ per FeSe unit. Our refinement indicated exclusively neutral ammonia molecules at the body-center of the unit cell as a total of 3.04(8) H/D atoms are located within a 1 Å radius of each N atom. Compared to the dissolved alkali metals in liquid ammonia, our hydrothermal conditions did not provide a strong enough reducing environment to stabilize $(ND_2)^-$ groups. Lack of an amide group may provide better stability

for ammonia-intercalated FeCh, which remained unchanged when exposed to air for days.

To verify the composition derived from diffraction studies, thermogravimetric analysis (TGA) was carried out. For $NH_{3.5}Fe_2Ch_2$, the combined contribution of nitrogen and hydrogen would be 9.04 wt% and 6.09 wt% for sulfide and selenide, respectively. These theoretical numbers are in good agreement with the results from TGA (Fig. S2, ESI†) where 9 wt% and 6 wt% losses were observed for sulfide and selenide, respectively.

Differential scanning calorimetry (DSC) provides a qualitative measure of the hydrogen bonding strength in these samples. For the sulfide sample, the abrupt weight loss near 300 °C was accompanied by a sharp endothermic transition in the DSC curve (Fig. S2a, ESI†). Therefore the thermal stability of $(H_{0.5}NH_3)Fe_2S_2$ exceeds by more than 100 °C that of tetragonal FeS before intercalation. FeS starts to decompose above 100 °C and completely converts to other sulfides near 200 °C.[25] The selenide is less stable as a gradual weight loss occurred between 150 and 300 °C (~5%) without any sharp transition in the DSC curve (Fig. S2b, ESI†). The initial decomposition temperature of $(H_{0.5}NH_3)Fe_2Se_2$ is fairly consistent with the Li·amine-intercalated FeSe, which decomposes around 100 °C.[3] However, the thermal stability of the two selenide phases diverges at higher temperature as the decomposition of $Li_{0.6}(ND_2)_{0.2}(ND_3)_{0.8}Fe_2Se_2$ is complete at 150 °C.[3]

The DSC results suggest that hydrogen bonding, especially between H^+ and Se^{2-} at the cell edges (2.491 Å), enhanced the overall stability of the structure. Such bonding seems to also be more effective for the smaller and more electronegative sulfur, where the S–H distance was 2.435 Å. Hence, the enhanced thermal stability of $NH_{3.5}Fe_2Ch_2$ can be attributed to stronger hydrogen bonds compared to other intercalated FeCh (2.6–3.1 Å) phases. Interestingly, the bond lengths in $(H_{0.5}NH_3)Fe_2S_2$ are comparable to Li·NH_3-intercalated TiS_2 with H(D)···S between 2.49 and 2.66 Å,[26] which decomposes above 200 °C.

Despite structural and chemical similarities to the Li·amine intercalated FeSe superconductor, neither $(H_{0.5}NH_3)Fe_2S_2$ nor $(H_{0.5}NH_3)Fe_2Se_2$ displays superconductivity. The lack of superconductivity may be a result of vacancies on the iron site (about 3(1)% from our NPD data) which is detrimental for the superconductivity of Fe chalcogenides.[3,12,14] For the sulfide sample, Curie-like paramagnetism was observed by magnetic susceptibility measurements (Fig. 3a). A Curie–Weiss fit gave a Curie constant C = 0.685 cm^3 K mol^{-1} and Weiss temperature Θ = −13.6 K. The effective magnetic moment (μ_{eff}) calculated based on the Curie constant is 2.33 μ_B, suggesting a spin state intermediate between S = 1/2 and S = 1 for Fe^{2+}. The effective moment is much smaller than high-spin (HS) Fe^{2+} with S = 2(4.9 μ_B) or Fe^{3+} with S = 5/2 A (5.9 μ_B). In contrast, μ_{eff} of Fe in non-superconducting $(Li_{1-x}Fe_xOH)FeS$ was found to be 4.98 μ_B,[18] which is in very good agreement with HS-Fe^{2+}. The smaller μ_{eff} of $(H_{0.5}{}^+NH_3)Fe_2S_2$ could be the result of mostly vacancy-free FeS layers and electron doping (~0.25e^-/Fe) by the protons.

Previously, we demonstrated that $(Li_{1-x}Fe_xOH)FeS$ could be tuned into a superconductor with optimal electron doping of 0.13e^-/Fe.[17] It is possible that over-doping of $(H_{0.5}NH_3)Fe_2S_2$ suppressed superconductivity by resulting in vacancies on the iron position. This

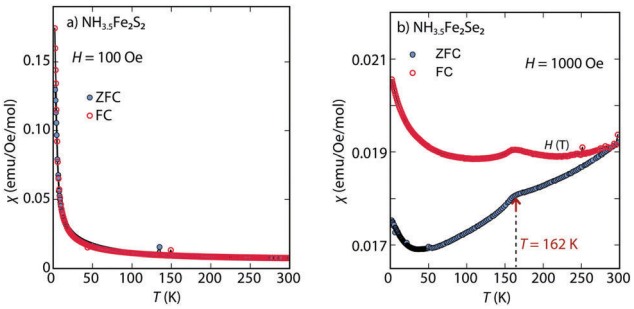

Fig. 3 Magnetic susceptibility of ammonia-intercalated (a) FeS and (b) FeSe, as a function of temperature. Zero-field cooled (ZFC) and field-cooled (FC) data are shown in blue and red, respectively. The molar susceptibility is calculated based on per mole iron.

occurs because Fe is over-reduced by the high amount of electron doping, and the formation of vacancies help re-oxidize iron up to Fe(II) as occurs in the vacancy-ordered $K_2Fe_4Se_5$ phase.[27] It is also likely that over-doping enhanced the covalent characters of Fe–S bonding, leading to a lower spin state for Fe^{2+}. The selenide analogue also displays paramagnetism (Fig. 3b), but its molar susceptibility is an order of magnitude smaller than that of the sulfide analogue. Due to some ferromagnetic impurity not detectable by PXRD, we did not carry out a Curie–Weiss analysis of $(H_{0.5}NH_3)Fe_2Se_2$. Interestingly, a cusp in the magnetic susceptibility near 162 K (Fig. 3) suggests that long-range antiferromagnetic ordering may be present in the selenide analogue. Further neutron diffraction studies would be interesting to know whether this over-doping regime (optimal for superconductivity is near 0.15–0.2e^-/Fe[6]) leads to an antiferromagnetic parent phase as found for the iron arsenide superconductors.

Electronic band structure calculations could enlighten our understanding of the magnetic properties and predict the electrical transport properties. It seems that the doping of electrons in $(H_{0.5}NH_3)Fe_2Ch_2$ leads to enhanced Fermi-surface nesting suggested by the two-dimensional electronic density of states (DOS) (Fig. S4, ESI†). The overall DOS and band structure are similar to those of FeCh, but larger electron pockets at the M-point were found for $(H_{0.5}NH_3)Fe_2Ch_2$. This also means that both compounds should be metallic in their electrical transport.

To further probe any interesting electronic behavior and possible structural distortion induced by intercalates, we performed electron diffraction (ED) using a transmission electron microscope (TEM). The ED patterns of both compounds show a clear square-lattice with no indication of structural distortion that would break the 4-fold symmetry (Fig. 4). However, forbidden reflections were observed at $h + k = 2n + 1$ for the sulfide analogue, which may be attributed to defects such as strain or stacking faults, common in layered materials.[28] For both samples, superlattice reflections with a vector $\vec{k}$ = (1/2, 1/2, 0) were also observed. A possible explanation for these extra reflections is a charge density wave (CDW) due to enhanced Fermi-surface nesting. Such CDWs have been observed in other phases proximate to superconductivity such as layered dichalcogenides.[29] Although it is unclear whether the true nature of the superlattice reflections is a CDW or other electronic instability, the likely cause is overdoping of electrons as superlattice reflections were not observed for the FeCh phases.[17]

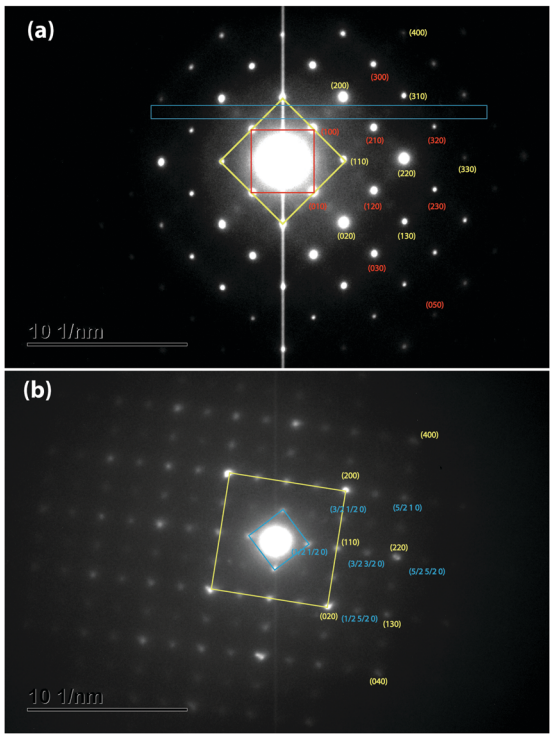

Fig. 4 Electron diffraction patterns of ammonia-intercalated (a) FeS and (b) FeSe. The allowed, forbidden and superlattice reflections are indicated in yellow, red and blue, respectively.

Finally, we explored the de-intercalation and cation exchange properties of $(H_{0.5}NH_3)Fe_2Ch_2$ to tune both the crystal structure and composition. From route **1** to **2** in Fig. 1, FeSe is easily afforded while FeS always contained some alkali hydroxide intercalated impurities. Interestingly, the de-intercalated FeSe is partially superconducting (T_c = 7 K as shown in Fig. S5, ESI†). Previously, FeSe prepared by direct hydrothermal routes was found to be not superconducting.[30] This would be the first time superconducting FeSe is prepared in aqueous solution. The only other solution-based method to afford superconducting FeSe was reaction of Fe with Se in ethylene glycol at 200 °C.[31]

We can then exchange the H^+ in $(H_{0.5}NH_3)Fe_2Ch_2$ by Li^+ by carrying out the reaction by topochemical conversion in liquid ammonia (**1** to **3** in Fig. 1). This would be the first preparation of $(Li_{0.5}NH_3)Fe_2S_2$ (Fig. S6, ESI†) and it displays magnetic susceptibility with a broad peak centered at 32 K (Fig. S7, ESI†). This lack of a clear cusp in the susceptibility could be indicative of short-range antiferromagnetism. By using LiOH for the conversion instead, the H^+ and NH_3 species are completely replaced by LiOH (Fig. S8, ESI†). These topochemical conversion reactions proved that $(H_{0.5}NH_3)Fe_2Ch_2$ is a versatile precursor for a variety of chemical manipulations. New emerging properties such as superconductivity and magnetic ordering may be induced by finer tuning of the electron doping into the FeCh layers.

Research at the University of Maryland was supported by the NSF Career DMR-1455118. We acknowledge the support of the National Institute of Standards and Technology, U.S. Department of Commerce, in providing the neutron research facilities and the University of Maryland supercomputing resources (http://www.it.umd.edu/hpcc).

Conflicts of interest

There are no conflicts to declare.

References

1 J. Guo, S. Jin, G. Wang, S. Wang, K. Zhu, T. Zhou, M. He and X. Chen, *Phys. Rev. B: Condens. Matter Mater. Phys.*, 2010, **82**, 180520.
2 T. P. Ying, X. L. Chen, G. Wang, S. F. Jin, T. T. Zhou, X. F. Lai, H. Zhang and W. Y. Wang, *Sci. Rep.*, 2012, **2**, 426.
3 M. Burrard-Lucas, D. G. Free, S. J. Sedlmaier, J. D. Wright, S. J. Cassidy, Y. Hara, A. J. Corkett, T. Lancaster, P. J. Baker, S. J. Blundell and S. J. Clarke, *Nat. Mater.*, 2013, **12**, 15–19.
4 X. F. Lu, N. Z. Wang, G. H. Zhang, X. G. Luo, Z. M. Ma, B. Lei, F. Q. Huang and X. H. Chen, *Phys. Rev. B: Condens. Matter Mater. Phys.*, 2014, **89**, 020507.
5 T. Ying, X. Chen, G. Wang, S. Jin, X. Lai, T. Zhou, H. Zhang, S. Shen and W. Wang, *J. Am. Chem. Soc.*, 2013, **135**, 2951–2954.
6 H. K. Vivanco and E. E. Rodriguez, *J. Solid State Chem.*, 2016, **242**, 3–21.
7 X. Zhou and E. E. Rodriguez, *Chem. Mater.*, 2017, **29**, 5737–5752.
8 T. Hatakeda, T. Noji, T. Kawamata, M. Kato and Y. Koike, *J. Phys. Soc. Jpn.*, 2013, **82**, 123705.
9 S. Hosono, T. Noji, T. Hatakeda, T. Kawamata, M. Kato and Y. Koike, *J. Phys. Soc. Jpn.*, 2014, **83**, 113704.
10 S. Jin, X. Fan, X. Wu, R. Sun, H. Wu, Q. Huang, C. Shi, X. Xi, Z. Li and X. Chen, *Chem. Commun.*, 2017, **53**, 9729–9732.
11 A. Krzton-Maziopa, E. V. Pomjakushina, V. Y. Pomjakushin, F. von Rohr, A. Schilling and K. Conder, *J. Phys.: Condens. Matter*, 2012, **24**, 382202.
12 S. J. Sedlmaier, S. J. Cassidy, R. G. Morris, M. Drakopoulos, C. Reinhard, S. J. Moorhouse, D. O'Hare, P. Manuel, D. Khalyavin and S. J. Clarke, *J. Am. Chem. Soc.*, 2014, **136**, 630–633.
13 J. W. Lynn, X. Zhou, C. K. H. Borg, S. R. Saha, J. Paglione and E. E. Rodriguez, *Phys. Rev. B: Condens. Matter Mater. Phys.*, 2015, **92**, 060510.
14 H. Sun, D. N. Woodruff, S. J. Cassidy, G. M. Allcroft, S. J. Sedlmaier, A. L. Thompson, P. A. Bingham, S. D. Forder, S. Cartenet, N. Mary, S. Ramos, F. R. Foronda, B. H. Williams, X. Li, S. J. Blundell and S. J. Clarke, *Inorg. Chem.*, 2015, **54**, 1958–1964.
15 X. Zhou, C. K. H. Borg, J. W. Lynn, S. R. Saha, J. Paglione and E. E. Rodriguez, *J. Mater. Chem. C*, 2016, **4**, 3934–3941.
16 J. T. Greenfield, C. Pak, S. Kamali, K. Lee and K. Kovnir, *Chem. Commun.*, 2015, **51**, 5355–5358.
17 X. Zhou, C. Eckberg, B. Wilfong, S.-C. Liou, H. K. Vivanco, J. Paglione and E. E. Rodriguez, *Chem. Sci.*, 2017, **8**, 3781–3788.
18 U. Pachmayr and D. Johrendt, *Chem. Commun.*, 2015, **51**, 4689–4692.
19 X. Zhou, B. Wilfong, H. Vivanco, J. Paglione, C. M. Brown and E. E. Rodriguez, *J. Am. Chem. Soc.*, 2016, **138**, 16432–16442.
20 C. Li, S. Sun, S. Wang and H. Lei, *Phys. Rev. B*, 2017, **96**, 134503.
21 B. Wilfong, X. Zhou, H. Vivanco, D. J. Campbell, K. Wang, D. Graf, J. Paglione and E. Rodriguez, *Phys. Rev. B*, 2018, **97**, 104408.
22 T. Yamada, X. Liu, U. Englert, H. Yamane and R. Dronskowski, *Chem. – Eur. J.*, 2009, **15**, 5651–5655.
23 S. Angyal and W. Warburton, *J. Chem. Soc.*, 1951, 2492–2494.
24 X. Zhou, W. Zhou, T. J. Udovic, T. Yildirim, J. J. Rush, E. E. Rodriguez and H. Wu, *Int. J. Hydrogen Energy*, 2016, **41**, 18542–18549.
25 A. R. Lennie, S. A. T. Redfern, P. E. Champness, C. P. Stoddart, P. F. Schofield and D. J. Vaughan, *Am. Mineral.*, 1997, 82.
26 V. Young Jr, M. McKelvy, W. Glaunsinger and R. Von Dreele, *Chem. Mater.*, 1990, **2**, 75–81.
27 D. P. Shoemaker, D. Y. Chung, H. Claus, M. C. Francisco, S. Avci, A. Llobet and M. G. Kanatzidis, *Phys. Rev. B: Condens. Matter Mater. Phys.*, 2012, **86**, 184511.
28 E. DiMasi, M. Aronson, J. Mansfield, B. Foran and S. Lee, *Phys. Rev. B: Condens. Matter Mater. Phys.*, 1995, **52**, 14516.
29 E. Morosan, H. Zandbergen, B. Dennis, J. Bos, Y. Onose, T. Klimczuk, A. Ramirez, N. Ong and R. Cava, *Nat. Phys.*, 2006, **2**, 544.
30 U. Pachmayr, N. Fehn and D. Johrendt, *Chem. Commun.*, 2016, **52**, 194–197.
31 J. T. Greenfield, S. Kamali, K. Lee and K. Kovnir, *Chem. Mater.*, 2015, **27**, 588–596.

